"Super-Heisenberg" and Heisenberg Scalings Achieved Simultaneously in the Estimation of a Rotating Field

Zhibo Hou,[1,2,*] Yan Jin,[1,2,*] Hongzhen Chen,[3] Jun-Feng Tang,[1,2] Chang-Jiang Huang,[1,2] Haidong Yuan,[3,†] Guo-Yong Xiang,[1,2,‡] Chuan-Feng Li,[1,2] and Guang-Can Guo[1,2]

[1]*CAS Key Laboratory of Quantum Information, University of Science and Technology of China, Hefei 230026, People's Republic of China*

[2]*CAS Center For Excellence in Quantum Information and Quantum Physics, University of Science and Technology of China, Hefei 230026, People's Republic of China*

[3]*Department of Mechanical and Automation Engineering, The Chinese University of Hong Kong, Shatin, Hong Kong SAR, China*

(Received 20 July 2020; accepted 25 January 2021; published 18 February 2021)

The Heisenberg scaling, which scales as N^{-1} in terms of the number of particles or T^{-1} in terms of the evolution time, serves as a fundamental limit in quantum metrology. Better scalings, dubbed as "super-Heisenberg scaling," however, can also arise when the generator of the parameter involves many-body interactions or when it is time dependent. All these different scalings can actually be seen as manifestations of the Heisenberg uncertainty relations. While there is only one best scaling in the single-parameter quantum metrology, different scalings can coexist for the estimation of multiple parameters, which can be characterized by multiple Heisenberg uncertainty relations. We demonstrate the coexistence of two different scalings via the simultaneous estimation of the magnitude and frequency of a field where the best precisions, characterized by two Heisenberg uncertainty relations, scale as T^{-1} and T^{-2}, respectively (in terms of the standard deviation). We show that the simultaneous saturation of two Heisenberg uncertainty relations can be achieved by the optimal protocol, which prepares the optimal probe state, implements the optimal control, and performs the optimal measurement. The optimal protocol is experimentally implemented on an optical platform that demonstrates the saturation of the two Heisenberg uncertainty relations simultaneously, with up to five controls. As the first demonstration of simultaneously achieving two different Heisenberg scalings, our study deepens the understanding on the connection between the precision limit and the uncertainty relations, which has wide implications in practical applications of multiparameter quantum estimation.

DOI: 10.1103/PhysRevLett.126.070503

Introduction.—The precision limit is fundamentally constrained by the resources, which are typically characterized by the number of probes (N) or the time (T). The optimal precision of classical strategies typically scales as $1/\sqrt{N}$ or $1/\sqrt{T}$ (in terms of the standard deviation) [1–5]. This is called the shot-noise limit [3,4,6]. By exploiting the quantum mechanical effects, such as superposition and entanglement, quantum metrology can achieve a precision that scales as $1/N$ or $1/T$ [7–20]. This is known as the Heisenberg scaling. With many-body interactions or time-dependent evolutions, however, it is possible to achieve precisions that scale as $1/N^k$ with $k > 1$ [21–31] or even exponentially [22]. This has been dubbed as super-Heisenberg scalings [21,23]. There has been some dispute about whether the super-Heisenberg scaling is really "super-Heisenberg" [22,24]. In [22], it has been shown that from the perspective of the query complexity the super-Heisenberg scalings are actually Heisenberg. This, both theoretically [21,22,26,30,31] and experimentally [23,25,27–29], has been restricted to the single-parameter quantum estimation so far, where there is only one optimal scaling.

Irrespective of the scaling, the precision limit can actually be characterized via the Heisenberg uncertainty relation, which justifies the name of the Heisenberg scaling. In the multiparameter quantum estimation [32–57], the best precision limits of different parameters can have different scalings, which can be characterized by different Heisenberg uncertainty relations. The interplay of multiple uncertainty relations, however, is little understood. Here we study the simultaneous saturation of two Heisenberg uncertainty relations related to the estimation of the amplitude and the frequency of a rotating magnetic field. By exploring the connections between the precision limits and the Heisenberg uncertainty relations, we show that it is possible to saturate the two uncertainty relations simultaneously, thus achieving two different scalings at the same time. This is achieved through the identification of the optimal probe state, the optimal controls employed during the evolution, and the optimal measurement on the evolved state. The identified optimal protocol provides the ultimate precision for the estimation of the two parameters simultaneously. We implement the protocol on an optical platform

and demonstrate the achievement of two different Heisenberg scalings simultaneously, with the precision of the estimation for the amplitude scaling as $1/T$ and the precision for the frequency scaling as $1/T^2$.

Precision limit characterized by the Heisenberg uncertainty relation.—The precision in quantum metrology is typically characterized by the quantum Cramer-Rao bound, a tool generalized from the classical statistics. This statistical tool, however, lacks a direct physical picture. A more fundamental tool is the Heisenberg uncertainty relation [58]. The connection between the precision limit and the uncertainty relation, however, has only received limited attention, mainly for the estimation of a single parameter x in the Hamiltonian of the form xH [59], where H is a parameter-independent Hermitian operator. We first illustrate this connection for the general unitary evolution and show that the achievement of the highest precisions for multiple parameters is equivalent to the saturation of multiple Heisenberg uncertainty relations simultaneously.

To estimate a parameter x encoded in a general unitary U_x, we can prepare an initial probe state $|\Psi_0\rangle$ and let it evolve under the unitary to get $|\Psi_x\rangle = U_x|\Psi_0\rangle$. The value of the parameter can then be estimated via proper measurement on the output state, described by an observable O_x. The precision of the estimation can then be quantified through the error propagation as

$$\delta x_{\text{est}} = \Delta O_x/|\partial_x\langle O_x\rangle|, \tag{1}$$

here $\Delta O_x = \sqrt{\Delta O_x^2}$ with $\Delta O_x^2 = \langle\Psi_x|O_x^2|\Psi_x\rangle - \langle\Psi_x|O_x|\Psi_x\rangle^2$, $\langle O_x\rangle = \langle\Psi_x|O_x|\Psi_x\rangle$, and $\delta x_{\text{est}} = \sqrt{E[(x_{\text{est}}-x)^2]}$ is the standard deviation of the estimator.

Let $h_x = i(\partial_x U_x)U_x^\dagger$ as the generator of the parameter [10,26,60,61], which plays a similar role as the Hamiltonian in Schrödinger's equation as $\partial_x|\Psi_x\rangle = -ih_x|\Psi_x\rangle$ and from $\partial_x(U_xU_x^\dagger) = 0$, it is also easy to see that $h_x = h_x^\dagger$. We then have

$$\partial_x\langle O_x\rangle = i\langle\Psi_x|[h_x, O_x]|\Psi_x\rangle. \tag{2}$$

From the Heisenberg uncertainty relation [58,59]

$$\Delta O_x\Delta h_x \geq \frac{1}{2}|\langle\Psi_x|[h_x, O_x]|\Psi_x\rangle| \tag{3}$$

and the connection between δx_{est} and O_x in Eq. (1), we can immediately get

$$\delta x_{\text{est}}\Delta h_x \geq \frac{1}{2}, \tag{4}$$

which leads to the bound on the precision as $\delta x_{\text{est}} \geq (1/2\Delta h_x)$. The optimal observable that saturates Eq. (3) should satisfy

$$(h_x - \langle h_x\rangle)|\Psi_x\rangle = i\gamma(O_x - \langle O_x\rangle)|\Psi_x\rangle. \tag{5}$$

We note that the time-energy uncertainty relation can be seen as a special example when x is taken as the time.

To achieve the minimum δx_{est}, we should (1) find the probe state that maximizes Δh_x^2 and (2) find the observable that saturates Eq. (3). For single-parameter quantum estimation, these conditions can always be satisfied to saturate one Heisenberg uncertainty relation. To achieve the best precisions for multiple parameters, however, multiple Heisenberg uncertainty relations need to be saturated, which may not be always possible.

Here we consider the simultaneous estimation of the amplitude and the frequency of a rotating magnetic field, where the interaction of the field with a probe spin can be described by the Hamiltonian

$$H(t) = -\mathbf{B}(t)\cdot\boldsymbol{\sigma} = -B(\cos\omega t\sigma_X + \sin\omega t\sigma_Z), \tag{6}$$

where B denotes the magnitude of the field and ω denotes the frequency of the rotation. The estimation of B or ω separately has been studied in the single-parameter estimation, where it has been shown that the best precision of B scales as $1/(2T)$ and the best precision of ω scales as $1/(BT^2)$ [26]. It is, however, not clear whether such precisions can be achieved simultaneously. The simultaneous achievement of these precisions requires the existence of (1) the same optimal probe state, (2) the same optimal control, and (3) compatible optimal measurements for both parameters.

To ease the identification of the optimal probe state, we calculate the variance of the generator in the Heisenberg picture as $\Delta[h_x^H(T)]^2_{|\Psi_0\rangle} = \Delta[h_x(T)]^2_{|\Psi_x\rangle}$, here $h_x^H(T) = U_x^\dagger(T)h_xU_x(T) = iU_x^\dagger(T)\partial_xU_x(T)$ with $U_x(T)$ as the generated unitary operator acting on the probe state. At any given time T the generator can be obtained as [60–62]

$$h_x^H(T) = \int_0^T U_x^\dagger(0\to t)\partial_xH(t)U_x(0\to t)dt. \tag{7}$$

For the parameter B, we have $\partial_BH(t) = -(\cos\omega t\sigma_X + \sin\omega t\sigma_Z)$ and for ω we have $\partial_\omega H(t) = Bt(\sin\omega t\sigma_X - \cos\omega t\sigma_Z)$. To understand the evolution of the generators in a geometrical way, we use the Bloch representation to write the generator at time T as $h_x^H(T) = \mathbf{S}_x(T)\cdot\boldsymbol{\sigma}$ and write $U_x^\dagger(0\to t)\partial_xH(t)U_x(0\to t) = \mathbf{V}_x(t)\cdot\boldsymbol{\sigma}$. Specifically, $\mathbf{S}_x(T)$ can be viewed as the accumulated displacement at time T and $\mathbf{V}_x(t)$ can be viewed as the instantaneous velocity with $\mathbf{S}_x^H(T) = \int_0^T\mathbf{V}_x(t)dt$. The largest standard deviation of the generator is upper bounded by the norm of $|\mathbf{S}_x^H(T)|$ as

$$\Delta h_x^H(T) \leq |\mathbf{S}_x^H(T)|, \tag{8}$$

and the norm of $|\mathbf{S}_x^H(T)|$ is further upper bounded as

$$|\mathbf{S}_x^H(T)| \le \int_0^T |\mathbf{V}_x(t)|dt = \int_0^T |\partial_x H(t)|dt, \quad (9)$$

where the last equality we used the fact that $|U_x^\dagger(0\to t)\partial_x H(t)U_x(0\to t)| = |\partial_x H(t)|$. Geometrically, this is in analogy to the fact that the displacement between two points is always upper bounded by the length of a path that connects them. Since $|\partial_B H(t)| = 1$ and $|\partial_\omega H(t)| = Bt$, we have $\Delta h_B^H(T) \le T$ and $\Delta h_\omega^H(T) \le \frac{1}{2}BT^2$. The best precision for the estimation of B or ω thus scales at most as T^{-1} or T^{-2}, respectively. The difference between them originates from the difference between the norm of the instantaneous velocity $|\mathbf{V}_x(t)|$, as there is an extra t in $\mathbf{V}_\omega(t)$ as compared to $\mathbf{V}_B(t)$.

To achieve the best precisions, we need to saturate the two inequalities in Eqs. (8) and (9). The inequality in Eq. (9), however, cannot be saturated under the free evolution in general, as it requires the instantaneous velocity $\mathbf{V}_x(t)$ aligned in the same direction during the whole evolution, which, in general, is not the case. Thus, under the free evolution, the scaling of T^{-1} and T^{-2} for the estimation of B and ω cannot be achieved simultaneously. Detailed calculation of the generators and their variances under the free evolution can be found in the Supplemental Material [63].

To achieve the best precision, we need to use quantum controls to tame the dynamics so that $\mathbf{V}_x(t)$ at different time points can be aligned. This can be achieved by adding a control term $H_c(t)$ to the Hamiltonian, $H_{\rm tot}(t) = H(t) + H_c(t)$. A choice of the control that can align the velocity [26] is

$$H_c(t) = B_c(\cos\omega_c t\sigma_X + \sin\omega_c t\sigma_Z) - \frac{\omega_c}{2}\sigma_Y, \quad (10)$$

with B_c and ω_c as the estimated value of B and ω, respectively, which need to be updated adaptively with the accumulation of the collected measurement results. When these estimates converge to the true value, i.e., when $B_c = B$ and $\omega_c = \omega$, $\mathbf{V}_B(t) = (-1, 0, 0)$ and $\mathbf{V}_\omega(t) = (0, 0, -Bt)$ at different t are completely aligned under the controlled dynamics and the best precision can then be achieved. This can be seen by directly calculating the generators under the controlled dynamics, which are given by

$$h_B^H(T)|_{B_c=B,\omega_c=\omega} = -T\sigma_X, \quad (11)$$

$$h_\omega^H(T)|_{B_c=B,\omega_c=\omega} = -\frac{1}{2}BT^2\sigma_Z. \quad (12)$$

Thus, $|\mathbf{S}_B^H(T)| = T$ and $|\mathbf{S}_\omega^H(T)| = BT^2/2$, both attain the maximal value.

The inequality in Eq. (8) can be saturated by optimizing the initial probe state $|\Psi_0\rangle$, which needs to be the same for both parameters. By employing an ancillary qubit, the optimal probe state can be taken as the maximally entangled state $|\Psi_0\rangle = (|00\rangle + |11\rangle)/\sqrt{2}$, where the basis $|0\rangle$ and $|1\rangle$ are the eigenstates of σ_Z with eigenvalues ± 1. It is easy to verify that this state saturates the inequalities in Eq. (8) for both parameters (see Supplemental Material [63]). At last, the optimal observables O_B and O_ω that saturate the two Heisenberg uncertainty relations associated with the two parameters need to commute with each other so the optimal measurements to achieve the best precision for the two parameters are compatible. It is easy to check that choosing the two observables in the Heisenberg picture as $O_B^H = \sigma_Y\sigma_Z$ and $O_\omega^H = \sigma_X\sigma_Y$ saturate Eq. (3) and they commute with each other (see Supplemental Material [63]). Thus, with the optimization of the probe state, the control, and the measurement, the best precision for the estimation of B and ω, which scales as T^{-1} and T^{-2}, respectively, can be achieved simultaneously.

Discrete controls.—In many physical settings, the controls are discrete rather than continuous, which is the case for our optical experiment. We thus use the discrete controls to approximate the optimal continuous control in the experiment. This can be achieved by dividing the total evolution time T into n small intervals, each with a duration $\delta t = T/n$, and a control is then added after each δt. For example, for the kth interval, the total dynamics is given by $U_{\rm tot}[(k-1)\delta t \to k\delta t] = C_k U[(k-1)\delta t \to k\delta t]$, where $U[(k-1)\delta t \to k\delta t]$ represents the free evolution during the interval, and C_k represents the added control. We note that $U_{\rm tot}[(k-1)\delta t \to k\delta t]$ not only depends on the time interval δt, but also depends on the starting time $(k-1)\delta t$ since the Hamiltonian is time dependent. In our experiment, the control operation C_k for the kth interval is generated by two operators as $C_k = U_{c1}U_{c2}$, where U_{c1} represents the operator generated from $H_1 = B_c(\cos\omega_c t\sigma_X + \sin\omega t\sigma_Z)$ and U_{c2} the operator generated from $H_2 = -(\omega_c/2)\sigma_X$ during the time interval $[(k-1)\delta t, k\delta t]$. The discrete control converges to the optimal continuous control when $n \to \infty$. We perform the simulation of the discrete control and show that, for the chosen evolution time, by dividing the total evolution into five intervals, the performance is already close to the optimal performance of the ideal optimal continuous control (see the Supplemental Material [63]).

Experimental setup.—We implement the protocol with a photonic system and demonstrate the simultaneous saturation of the two different scalings. The experiment setup consists of three modules: preparation, evolution, and measurement, as shown in Fig. 1(b). In the module of the preparation, we use the polarization of the photon as the probe system, where the horizontal (H) and vertical (V) polarization are taken as the basis, and the path degrees of the photon as the ancilla, where the up and down path are taken as the basis. We use a 40-mW H-polarized beam at 404 nm to pump a 1-mm-long BBO crystal, cut for type-I phase-matched spontaneous parametric down-conversion

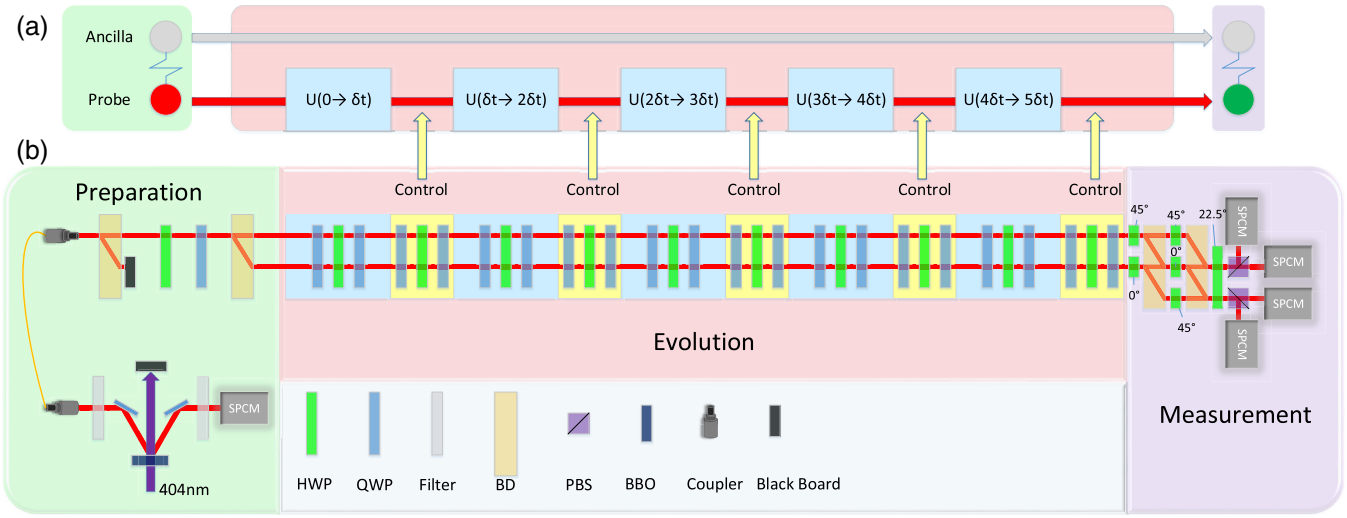

FIG. 1. Control-enhanced scheme and experimental setup. (a) Control-enhanced scheme. An ancilla-assisted state $1/\sqrt{2}(|00\rangle + |11\rangle)$ is prepared. The probe state undergoes five periods unitary evolution and five controls. (b) Experimental setup. There are three modules in the experiment: state preparation, evolution, and measurement. The state preparation prepares probe-ancilla state $(|H, \text{down}\rangle + |V, \text{up}\rangle)/\sqrt{2}$ in the degree of polarization and path of a heralded single photon. In the evolution module, the probe qubit is operated by the unknown U and the adaptive control U_c for n times ($n = 5$ in the figure and experiment). In the measurement module, projective measurements on the common eigenstates of $\sigma_Y\sigma_Z$ and $\sigma_X\sigma_Y$ are performed on the probe and ancilla to extract information of U. β-barium borate (BBO).

process, to generate a heralded single photon [64] at the rate of 3500 Hz. After passing through a beam displacer (BD), a half-wave plate (HWP), and a quarter-wave plate (QWP), the photon is prepared in the state $(|H\rangle + |V\rangle)/\sqrt{2}$. After passing through the second BD, the V component is displaced to the down path and the H component remains in the up path; this prepares the two degrees of the photon and prepares the initial state as $(|H, \text{down}\rangle + |V, \text{up}\rangle)/\sqrt{2}$. In the module of the evolution, the operations of the free evolution and the control are performed on the polarization qubit (probe), while the path qubit is unchanged (ancilla). The free evolution (blue) during a period δt and the control (yellow) are experimentally realized with a combination of two QWPs and one HWP, which can be used to generate arbitrary unitary operations on a polarization qubit. Overall, we use ten sets of such combinations of wave plates to generate five operators corresponding to the free evolution and another five operators corresponding to the control operation. In the module of the measurement, the projective measurement on the common eigenstates of $\sigma_Y\sigma_Z$ and $\sigma_X\sigma_Y$ are performed on the probe and ancilla qubits using two BDs, two polarization beam splitters (PBSs), and six HWPs with nontrivial rotation angles specified in Fig. 1(b). The measurement results are recorded by four single-photon counting modules (SPCMs).

Experiment result.—We demonstrate the scaling of the precision for the estimation of B and ω with respect to the evolution time T. In the experiment, the total T is divided into five intervals, each with $\delta t = T/5$ and a control is added after each interval. We consider the sensitivity of the local estimation where B and ω are within a small neighborhood of known values. In this case, the optimal controls can be achieved at $B_c = B$ and $\omega_c = \omega$. We note that, if the values of the parameters are completely unknown, by adaptively updating the controls with the accumulated measurement data, the control can always converge to the optimal ones. We implement the protocol with 1000 photons and collect the measurement outcomes from the four detectors. The estimators B_{est} and ω_{est} are then obtained with the maximum likelihood, which maximizes the posterior probability based on the obtained data. We repeat this process 200 times to get the distribution and the standard deviations of B_{est} and ω_{est}. In the experiment, we choose $T = 0.15 \times 5^{k/7}$ with $k = 1, 2, \ldots, 7$; i.e., T ranges from 0.19 to 0.75. It can be seen that the obtained precisions (blue and red dots in Fig. 2) for the estimation of B and ω achieve the best scaling of T^{-1} and T^{-2}, respectively, which matches the theoretical prediction.

Summary.—We experimentally achieved two different Heisenberg scalings, T^{-1} and T^{-2}, simultaneously for a multiparameter quantum estimation through the optimal design of the probe state, the control, and the measurement. Our Letter not only provides the ultimate precision on the simultaneous estimation of both the magnitude and the frequency of a field, which has wide implications in quantum magnetometry, quantum gyroscope, and spectroscope. It also deepens the connection between quantum metrology and the Heisenberg uncertainty relations, two

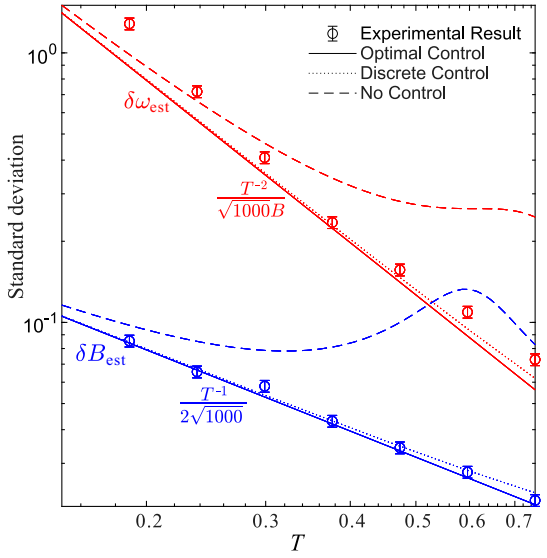

FIG. 2. Experimental results of the standard deviation of B and ω in the simultaneous estimation. In the experiment, parameters are $B = 1$, $\omega = 10$, $B_c = 1$, $\omega_c = 10$, $\delta t = T/5$. The numerical simulation for the performance under the dynamics with the optimal continuous control, the discrete control, and without control are plotted together with the experimental results with the discrete control. The procedure is repeated with 1000 times, which leads to the theoretical benchmark for the best precision of $B_{\rm est}$ as $[1/(2\sqrt{1000}T)]$ and the best precision of $\omega_{\rm est}$ as $[1/(\sqrt{1000}BT^2)]$.

fields that have been developed without sufficient crosses [65]. Our results strengthen the connections that shed light on the studies of both fields.

The work at U.S. T. C. is supported by the National Natural Science Foundation of China under Grants No. 61905234, No. 11974335, No. 11574291, and No. 11774334, the National Key Research and Development Program of China (No. 2017YFA0304100 and No. 2018YFA0306400), Key Research Program of Frontier Sciences, CAS (No. QYZDY-SSW-SLH003), and the Fundamental Research Funds for the Central Universities (No. WK2470000026). The work at C. U. H. K. is supported by Research Grants Council of Hong Kong (GRF No. 14308019), Research Strategic Funding Scheme of CUHK (Grant No. 3133234).

*These authors contributed equally to this work.
†hdyuan@mae.cuhk.edu.hk
‡gyxiang@ustc.edu.cn

[1] C. W. Helstrom, *Quantum Detection and Estimation Theory* (Academic Press, New York, 1976).
[2] A. S. Holevo, *Probabilistic and Statistical Aspects of Quantum Theory* (North-Holland, Amsterdam, 1982).
[3] C. M. Caves, Phys. Rev. D **23**, 1693 (1981).
[4] B. Yurke, S. L. McCall, and J. R. Klauder, Phys. Rev. A **33**, 4033 (1986).
[5] R. Demkowicz-Dobrzański, M. Jarzyna, and J. Kołodyński, in *Progress in Optics* (Elsevier, New York, 2015), Vol. 60, pp. 345–435.
[6] M. G. Paris, Int. J. Quantum. Inform. **07**, 125 (2009).
[7] M. W. Mitchell, J. S. Lundeen, and A. M. Steinberg, Nature (London) **429**, 161 (2004).
[8] P. Walther, J.-W. Pan, M. Aspelmeyer, R. Ursin, S. Gasparoni, and A. Zeilinger, Nature (London) **429**, 158 (2004).
[9] V. Giovannetti, S. Lloyd, and L. Maccone, Science **306**, 1330 (2004).
[10] V. Giovannetti, S. Lloyd, and L. Maccone, Phys. Rev. Lett. **96**, 010401 (2006).
[11] T. Nagata, R. Okamoto, J. L. O'brien, K. Sasaki, and S. Takeuchi, Science **316**, 726 (2007).
[12] B. L. Higgins, D. W. Berry, S. D. Bartlett, H. M. Wiseman, and G. J. Pryde, Nature (London) **450**, 393 (2007).
[13] G. Y. Xiang, B. L. Higgins, D. W. Berry, H. M. Wiseman, and G. J. Pryde, Nat. Photonics **5**, 43 (2011).
[14] V. Giovannetti, S. Lloyd, and L. Maccone, Nat. Photonics **5**, 222 (2011).
[15] S. Slussarenko, M. M. Weston, H. M. Chrzanowski, L. K. Shalm, V. B. Verma, S. W. Nam, and G. J. Pryde, Nat. Photonics **11**, 700 (2017).
[16] S. Daryanoosh, S. Slussarenko, D. W. Berry, H. M. Wiseman, and G. J. Pryde, Nat. Commun. **9**, 4606 (2018).
[17] H. Yuan and C.-H. F. Fung, npj Quantum Inf. **3**, 14 (2017).
[18] Z. Hou, R.-J. Wang, J.-F. Tang, H. Yuan, G.-Y. Xiang, C.-F. Li, and G.-C. Guo, Phys. Rev. Lett. **123**, 040501 (2019).
[19] D. Braun, G. Adesso, F. Benatti, R. Floreanini, U. Marzolino, M. W. Mitchell, and S. Pirandola, Rev. Mod. Phys. **90**, 035006 (2018).
[20] J. S. Sidhu and P. Kok, AVS Quantum Sci. **2**, 014701 (2020).
[21] S. Boixo, A. Datta, M. J. Davis, S. T. Flammia, A. Shaji, and C. M. Caves, Phys. Rev. Lett. **101**, 040403 (2008).
[22] M. Zwierz, C. A. Pérez-Delgado, and P. Kok, Phys. Rev. Lett. **105**, 180402 (2010).
[23] M. Napolitano, M. Koschorreck, B. Dubost, N. Behbood, R. Sewell, and M. W. Mitchell, Nature (London) **471**, 486 (2011).
[24] M. J. W. Hall and H. M. Wiseman, Phys. Rev. X **2**, 041006 (2012).
[25] R. J. Sewell, M. Napolitano, N. Behbood, G. Colangelo, F. Martin Ciurana, and M. W. Mitchell, Phys. Rev. X **4**, 021045 (2014).
[26] S. Pang and A. N. Jordan, Nat. Commun. **8**, 14695 (2017).
[27] J. M. Boss, K. Cujia, J. Zopes, and C. L. Degen, Science **356**, 837 (2017).
[28] S. Schmitt, T. Gefen, F. M. Stürner, T. Unden, G. Wolff, C. Müller, J. Scheuer, B. Naydenov, M. Markham, S. Pezzagna *et al.*, Science **356**, 832 (2017).
[29] M. Naghiloo, A. N. Jordan, and K. W. Murch, Phys. Rev. Lett. **119**, 180801 (2017).
[30] M. M. Rams, P. Sierant, O. Dutta, P. Horodecki, and J. Zakrzewski, Phys. Rev. X **8**, 021022 (2018).
[31] T. Gefen, A. Rotem, and A. Retzker, Nat. Commun. **10**, 4992 (2019).
[32] J. Kahn, Phys. Rev. A **75**, 022326 (2007).

[33] H. Imai and A. Fujiwara, J. Phys. A **40**, 4391 (2007).
[34] M. A. Ballester, Phys. Rev. A **70**, 032310 (2004).
[35] P. J. D. Crowley, A. Datta, M. Barbieri, and I. A. Walmsley, Phys. Rev. A **89**, 023845 (2014).
[36] P. C. Humphreys, M. Barbieri, A. Datta, and I. A. Walmsley, Phys. Rev. Lett. **111**, 070403 (2013).
[37] X.-X. J. Jing Liu and X. Wang, Sci. Rep. **5**, 8565 (2015).
[38] N. Liu and H. Cable, Quantum Sci. Technol. **2**, 025008 (2017).
[39] T. Baumgratz and A. Datta, Phys. Rev. Lett. **116**, 030801 (2016).
[40] M. Szczykulska, T. Baumgratz, and A. Datta, Adv. Phys. X **1**, 621 (2016).
[41] H. Yuan, Phys. Rev. Lett. **117**, 160801 (2016).
[42] Y. Chen and H. Yuan, New J. Phys. **19**, 063023 (2017).
[43] S. Ragy, M. Jarzyna, and R. Demkowicz-Dobrzański, Phys. Rev. A **94**, 052108 (2016).
[44] M. D. Vidrighin, G. Donati, M. G. Genoni, X.-M. Jin, W. S. Kolthammer, M. S. Kim, A. Datta, M. Barbieri, and I. A. Walmsley, Nat. Commun. **5**, 3532 (2014).
[45] R. D. Gill and S. Massar, Phys. Rev. A **61**, 042312 (2000).
[46] E. Bagan, M. A. Ballester, R. D. Gill, R. Muñoz-Tapia, and O. Romero-Isart, Phys. Rev. Lett. **97**, 130501 (2006).
[47] N. Li, C. Ferrie, J. A. Gross, A. Kalev, and C. M. Caves, Phys. Rev. Lett. **116**, 180402 (2016).
[48] H. Zhu and M. Hayashi, Phys. Rev. Lett. **120**, 030404 (2018).
[49] Z. Hou, Z. Zhang, G.-Y. Xiang, C.-F. Li, G.-C. Guo, H. Chen, L. Liu, and H. Yuan, Phys. Rev. Lett. **125**, 020501 (2020).
[50] X.-Q. Zhou, H. Cable, R. Whittaker, P. Shadbolt, J. L. O'Brien, and J. C. Matthews, Optica **2**, 510 (2015).
[51] M. A. Ciampini, N. Spagnolo, C. Vitelli, L. Pezzè, A. Smerzi, and F. Sciarrino, Sci. Rep. **6**, 28881 (2016).
[52] E. Roccia, I. Gianani, L. Mancino, M. Sbroscia, F. Somma, M. G. Genoni, and M. Barbieri, Quantum Sci. Technol. **3**, 01LT01 (2018).
[53] Z. Hou, J.-F. Tang, J. Shang, H. Zhu, J. Li, Y. Yuan, K.-D. Wu, G.-Y. Xiang, C.-F. Li, and G.-C. Guo, Nat. Commun. **9**, 1414 (2018).
[54] E. Polino, M. Riva, M. Valeri, R. Silvestri, G. Corrielli, A. Crespi, N. Spagnolo, R. Osellame, and F. Sciarrino, Optica **6**, 288 (2019).
[55] F. Albarelli, M. Barbieri, M. G. Genoni, and I. Gianani, Phys. Lett. A **384**, 126311 (2020).
[56] H. Chen and H. Yuan, Phys. Rev. A **99**, 032122 (2019).
[57] J. Liu, H. Yuan, X.-M. Lu, and X. Wang, J. Phys. A **53**, 023001 (2020).
[58] W. Heisenberg, Z. Phys. **43**, 172 (1927).
[59] S. L. Braunstein, C. M. Caves, and G. J. Milburn, Ann. Phys. (N.Y.) **247**, 135 (1996).
[60] S. Pang and T. A. Brun, Phys. Rev. A **90**, 022117 (2014).
[61] D. Brody and E.-M. Graefe, Entropy **15**, 3361 (2013).
[62] A. Wilce, arXiv:0912.5530.
[63] See Supplemental Material at http://link.aps.org/supplemental/10.1103/PhysRevLett.126.070503 for detailed analysis of the optimality of the protocol.
[64] P. G. Kwiat, E. Waks, A. G. White, I. Appelbaum, and P. H. Eberhard, Phys. Rev. A **60**, R773 (1999).
[65] Z. Hou, J.-F. Tang, H. Chen, H. Yuan, G.-Y. Xiang, C.-F. Li, and G.-C. Guo, Sci. Adv. **7**, eabd2986 (2021).